Effects of Au nanoparticles on the magnetic and transport properties of $La_{0.67}Sr_{0.33}MnO_3$ ultrathin layers

S. Brivio,[1] C. Magen,[2,*] A. A. Sidorenko,[3] D. Petti,[1] M. Cantoni,[1] M. Finazzi,[1] F. Ciccacci,[1] R. De Renzi,[3] M. Varela,[2] S. Picozzi,[4] and R. Bertacco[1]

[1]*LNESS, Dipartimento di Fisica, Politecnico di Milano, via Anzani 42, 22100 Como, Italy*

[2]*Oak Ridge National Laboratory, Oak Ridge, Tennessee 37830, USA*

[3]*Dipartimento di Fisica e Unità CNISM di Parma, Università degli Studi di Parma, V.le G.P. Usberti 7/A, 43124 Parma, Italy*

[4]*CASTI Regional Laboratory, CNR-INFM, Coppito, 67010 L'Aquila, Italy*

(Received 12 November 2009; revised manuscript received 25 January 2010; published 10 March 2010)

The effect of the proximity of Au nanoparticles on the transport and magnetic properties of ultrathin $La_{2/3}Sr_{1/3}MnO_3$ (LSMO) films has been investigated. We find a huge increase in the resistivity of the manganite (by four orders of magnitude for a Au nominal thickness of 2 nm), which is accompanied by a strong decrease in the Curie temperature. A combined scanning transmission electron microscopy and electron energy-loss spectroscopy analysis shows that interfaces are coherent and atomically sharp, and that the structural quality is very high. On the other hand, a strong reduction in the Mn oxidation state is seen upon Au capping. NMR data show a strong attenuation of the double exchange signal upon formation of Au nanoparticles. *Ab initio* calculations indicate a negligible influence of Au on LSMO at an ideal interface, with the LSMO surface magnetic and electronic properties essentially unchanged upon creation of the Au/LSMO interface. In view of these calculations, the experimental results cannot be explained in terms of purely electrostatic effects induced by the proximity of a noble metal. Here we propose that the main driving force underlying the observed change in physical properties is the high reactivity of Au nanoparticles, which can locally pump oxygen from the manganite, thus favoring a phase separation ensuing from O inhomogeneity which deteriorates the transport and electrical properties.

DOI: 10.1103/PhysRevB.81.094410 PACS number(s): 75.47.Lx, 68.55.−a, 68.37.Ma, 76.60.−k

I. INTRODUCTION

The ferromagnetic metallic oxide $La_{0.67}Sr_{0.33}MnO_3$ (LSMO) is a system with very complex and rich physics, whose electronic and magnetic properties may be altered by applying various perturbations such as electric and magnetic fields, strain, light, etc.[1] The high degree of spin polarization and colossal magnetoresistance make manganese perovskites, in particular the optimally doped ferromagnetic manganite LSMO, appealing ingredients for spintronic devices.[2–4] Such devices are based on heterostructures that involve contact of thin manganite LSMO layers with another material, e.g., superconductors, insulators, organic materials, and normal metals.[5–9]

In such heterostructures new phenomena can arise from the interfacial interaction[1] and the properties of thin LSMO layers are significantly different from those of the bulk. It is well established now, for instance, that strain strongly affects the bandwidth of LSMO thin films, depressing their metallic properties and giving rise to phase separation and the formation of a so-called dead layer at the interface with the substrate.[10–12] In some cases, the suppression of the double-exchange (DE) mechanism due to the orbital reconstruction is evident.[13,14] Likewise, it is reasonable to assume that for such heterostructures the electronic and magnetic properties of LSMO layers at the interface could be strongly affected by a conductive overlayer. Besides possible chemical effects arising from interfacial mixing, the creation of an interface with a noble metal could affect the electronic environments of manganites, changing basic electronic parameters such as the Hubbard energy, the electronic bandwidth, or the exchange energies by analogy with the case of Ag films on NiO.[15] Under this assumption, thin manganite films may be particularly suitable for devices where transport and magnetic properties could be tuned by an externally applied electric field and indeed much work has been done in this direction. Pallecchi *et al.*[16] demonstrated a shift of a few kelvin of the peak of the resistivity of LSMO in a lateral field effect device while very recently Triscone and co-workers[17] showed a change in the magnetization of LSMO at the interface with $PbZr_{0.2}Ti_{0.8}O_3$ under different conditions of dielectric polarization of the latter. Recently, it has been shown that the deposition of Au on top of a 4-nm-thick LSMO film produces a dramatic reduction in the Curie temperature ($\Delta T_C \sim 188$ K) with respect to uncoated LSMO films of the same thickness and reduces the value of the saturation magnetization.[18,19] A sizable T_C reduction (~ 60 K) was also observed when an inert $SrTiO_3$ (STO) layer was inserted between the gold film and the 4-nm-thick manganite layer, suggesting that this effect might have an electrostatic origin. Indeed, a depletion of charge at the $Ag/STO/La_{0.67}Ca_{0.33}MnO_3$ interfaces and effects on phase separation in the manganite were also demonstrated in Ref. 20.

In order to disentangle true electrostatic phenomena from other spurious effects, we have carried out a detailed investigation of the transport, magnetic, chemical, and structural properties of the Au/LSMO interface, combined with an *ab initio* study of the change induced by the proximity of Au in the manganite electronic properties. The general picture arising is that pure electrostatic effects (charge accumulation in the LSMO layer producing a sizable change in the doping or

screening of Coulomb interactions due to image charges in the Au layer) cannot account for the observed phenomena. On the other hand, the huge reduction in the Mn oxidation state (Mn OS) seen by electron energy-loss spectroscopy (EELS) in films capped with Au suggests the creation of oxygen vacancies. Thought Au is a chemically inert material, we propose that the high reactivity of Au nanoparticles is the driving force for a local oxygen pumping action producing a small concentration of oxygen vacancies, i.e., an average composition $La_{0.67}Sr_{0.33}MnO_{3-\delta}$, with δ up to 0.19 for LSMO films in direct contact with Au. The huge deterioration of the transport and magnetic properties is then interpreted in terms of an enhancement of the phase separation in the manganite film, essentially ensuing from the formation of nanoparticles at the early stage of growth of the Au overlayer.

II. EXPERIMENTAL AND COMPUTATIONAL DETAILS

LSMO single-crystal films with thickness ranging from 4 to 12 nm were grown by pulsed laser deposition on STO substrates and then capped with a 1- or 2-nm-thick gold layer by molecular-beam epitaxy. Details on the growth conditions are reported in Ref. 18.

In-plane magnetization was measured by using a commercial superconducting quantum interference device (SQUID), 5 T Quantum Design MPMS, in a magnetic field of 100 Oe. We avoided spurious contributions to the measured signal, other than those from the film and the substrate, by using diamagnetic sample holders with uniform mass and magnetic-moment distribution along the whole SQUID scanning length. The magnetization data of the manganite films were corrected for the observed diamagnetic contribution of the substrate and the top gold layers. Resistance measurements as a function of temperature were performed with a standard four points probe apparatus without patterning the film, with probes disposed on top of the films/heterostructures. A Keithley 2601 was used as a current source injecting a constant current of 100 nA and the resistivity values have been extracted according to the Van der Pauw relations from the knowledge of the film thickness.

Zero-field ^{55}Mn NMR spectra were collected with the home-built broadband fast-averaging NMR spectrometer HyReSpect[21] on a tuned probe circuit at $T=1.6$ K. The ^{55}Mn NMR spectra were obtained by Fourier transforming two pulse sequences. The plotted NMR spectra are always corrected rescaling their amplitudes by ω^2 and the enhancement factor η.[22] Scanning transmission electron microscopy (STEM)-EELS experiments were carried out in a VG Microscopes HB501UX dedicated STEM operated at 100 kV and equipped with an Enfina spectrometer and a Nion aberration corrector. Principal component analysis was used to remove random noise from the EEL spectra.

Ab initio calculations of the Au/LSMO interface have been performed within the generalized gradient approximation to the exchange-correlation potential within density-functional theory (DFT) using Vienna *ab initio* simulation package[23] and the projector-augmented-wave pseudopotentials. The plane-wave energy cutoff was set to 450 eV. The Brillouin zone was sampled with a $10\times10\times1$ Monkhorst-Pack grid[24] while the density of states (DOS) was calculated using the tetrahedron method with Blöchl corrections[25] and 100 k points.

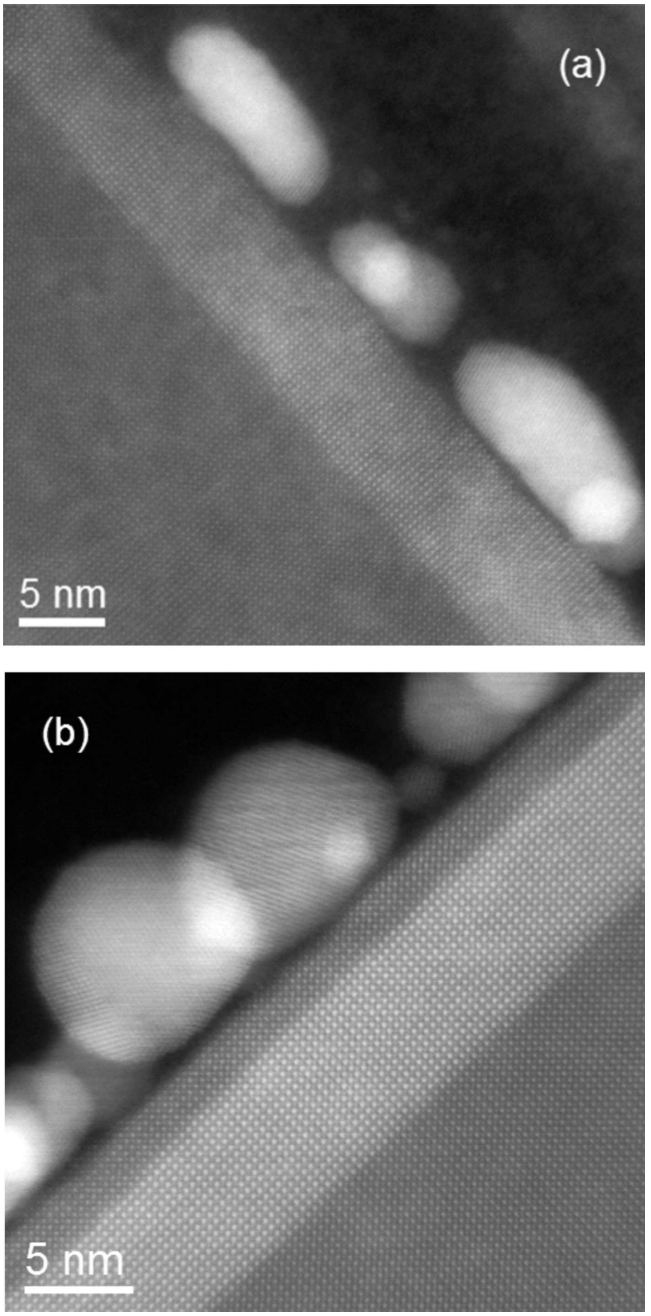

FIG. 1. Panel (a): ADF STEM image of Au nanoparticles on LSMO(6 nm)/STO(001). Panel (b): ADF STEM image of Au nanoparticles on STO(2 nm)/LSMO(6 nm)/STO(001).

III. EXPERIMENTAL RESULTS

A. STEM

Figure 1(a) presents a high-resolution annular dark field (ADF) STEM image (Z contrast) from a slice of a sample with the following structure: Au(2 nm)/LSMO(6 nm)//

STO(001). Apart from the high crystallinity of the LSMO film, this analysis clearly shows the formation of Au nanoparticles on top of LSMO for a nominal thickness of 2 nm of gold. As a matter of fact, only for nominal thickness above 8 nm the Au layer becomes continuous, as indicated by STEM and resistivity measurements (data not shown). Below this 8 nm critical value an island-growth mode occurs. This behavior most likely results from the higher value of the sum of the surface free energy of Au (γ_{Au}) and of the Au/LSMO interface (γ_{int}), with respect to the surface free energy of the LSMO free layer (γ_{LSMO}). In particular, the high value of the contact angle (>90°) indicates that $\gamma_{int} > \gamma_{LSMO}$, which is indeed related to the low tendency to form stable chemical bonds between Au and LSMO. This finding was already deduced from previous x-ray photoemission spectroscopy (XPS) investigation of the Au/LSMO interfaces[26] and is corroborated by chemical profiles obtained by EELS with atomic resolution, showing essentially no reaction or intermixing at this interface.[27]

The nanoparticles have spherical or ellipsoidal shape, without clear faceting or exposition of preferential crystallographic planes, and present an average lateral size on the order of 5–6 nm. The average height is ~4 nm, to be compared with 2 nm of nominal thickness, so that approximately 50% of the LSMO film is covered by Au particles. ADF images show that Au nanoparticles are polycrystalline with no clear preferential orientation of the Au atomic chains with respect to the substrate. This is more clearly seen in Fig. 1(b), where we present the case of Au nanoparticles on top of a 2 nm STO buffer layer inserted between Au and LSMO. In the biggest particle, atomic chains are seen in the left upper part of the particle, forming ~60° with the LSMO surface, which could be compatible with the structure of Au(111) planes. However in the same particle a clear dislocation is visible and in the neighbor particle on the right the orientation of atomic chains is completely different. These findings clearly indicate that strain effects induced on the LSMO films[28] by Au capping that could justify strong variations in the LSMO properties are of minor relevance, as the surface of contact is limited and there is no preferential epitaxial relation between Au nanoparticles and LSMO.

B. SQUID and transport measurements

The temperature dependence of the reduced magnetization measured in different heterostructures in a magnetic field of 100 Oe is shown in Fig. 2. The Curie temperature (T_C) obtained as the temperature corresponding to the higher temperature inflexion point of $M(T)$ decreases with the film thickness as expected for thin magnetic films: 325 ± 5 K for 6-nm-thick LSMO film (full circles) and 280 ± 5 K for 4-nm-thick LSMO film (full squares). A very relevant lowering (~185 ± 11 K) of the T_C is found after depositing a 2-nm-thick gold layer on top of the 4 nm LSMO film (see open squares in Fig. 2) while for the 6-nm-thick LSMO film the T_C reduction is much smaller (~10 ± 3 K) but is still clearly seen (open circles). The effect of the gold layer deposition on T_C, as measured by SQUID) disappears completely when the thickness of the manganite layer exceeds 8 nm.

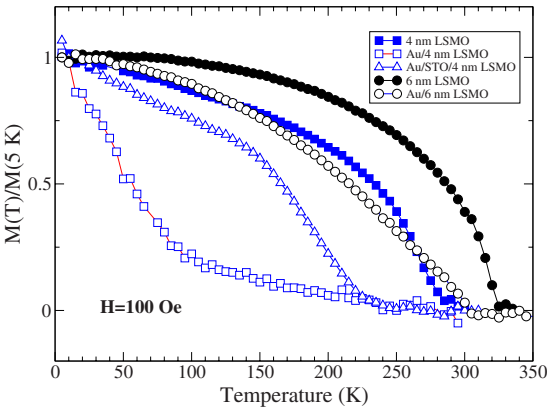

FIG. 2. (Color online) Normalized magnetization vs temperature measured at 100 Oe in different heterostructures. The thickness both of the gold layer and of the STO buffer layer is 2 nm.

This finding suggests that the phenomenon is limited to an interfacial layer. In addition, we inserted a chemically inert STO buffer layer between the gold layer and manganite film in order to hinder possible chemical reactions between Au and LSMO. Blue triangles in Fig. 2 display the temperature dependence of the magnetization of a Au(2 nm)/STO(2 nm)/LSMO(4 nm) heterostructure measured in a magnetic field of 100 Oe. In spite of the introduction of such STO buffer layer, a sizable decrease in the T_C ($\Delta T_C \sim 60$ K) is still found. It should be noted that the magnetization measurements of similar STO/LSMO/STO heterostructures without gold did not reveal any effect of a thin STO buffer layer on the magnetic properties of the LSMO layer.[18] The observed decrease in T_C is then effectively related to the presence of the Au overlayer on top.

In Fig. 3 the resistivity curves for a 4-nm-thick LSMO films (squares) and the heterostructures Au(1 nm)/LSMO(4 nm) (circles) and Au(2 nm)/LSMO(4 nm) (triangles) are shown. The overall behavior of the resistivity as a function of temperature was essentially independent on the current for intensities in the order of a few hundred of nanoampere. The 4-nm-thick LSMO film without gold displays a metal-insulator transition temperature (T_P) and resistivity values typical of films of this thickness.[16] A gold capping layer of 1

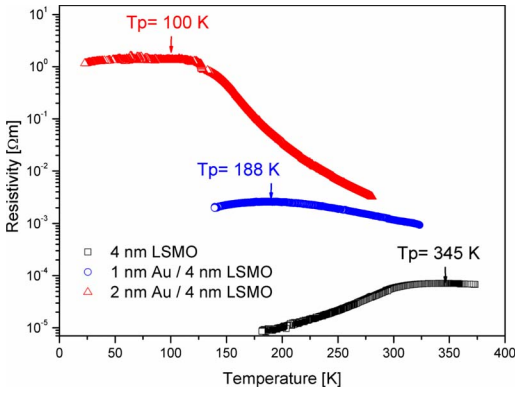

FIG. 3. (Color online) Resistivity as a function of temperature for 4 nm LSMO (squares), 1 nm Au/4 nm LSMO (circles) and 2 nm Au/4nm LSMO (triangles).

nm produces a strong increase in the peak resistivity (more than one order of magnitude) and a shift of the metal-insulator transition to lower temperatures (by 160 K). With a 2 nm capping layer the effects are even larger: the critical temperature is further reduced (down to 100 K) and the peak resistivity value is raised by about four orders of magnitude with respect to the free LSMO film. T_P is distinct from T_C, as observed also in thicker samples[29] but they correlate with each other and they are both drastically reduced with Au capping. The progressive increase in resistivity with nominal Au thickness reflects the formation of a discontinuous Au layer made of nanoparticles which does not shunt the manganite, thus allowing the measurement of its sheet resistance.

C. NMR

To determine the microscopic origin of changes in the magnetic behavior of the LSMO film ensuing from the addition of the gold layer, we have carried out zero-field ^{55}Mn NMR experiments. It is very well established that in the mixed-valence manganites different manganese states yield distinct contributions to the NMR spectra. The localized Mn^{4+} state gives rise to a peak between 310 and 330 MHz, whereas localized Mn^{3+} resonance varies between 350 and 430 MHz. The signal from the mixed-valence metallic region (Mn^{DE}, double-exchange state) is associated with a fast hopping of electrons among Mn sites and it shows up as a relatively narrow peak at an intermediate frequency in the 370–400 MHz range.[30–33]

Figure 4 shows the ^{55}Mn NMR spectra (solid lines represent the best fit) that we collected from several heterostructures with and without the gold overlayer. In all spectra at least two distinct lines at $f^{4+} \approx 322$ MHz and $f^{DE} \approx 376$ MHz are observed which can be attributed to two different phases with the localized charges (Mn^{4+} state) and with itinerant carriers (Mn^{DE} state), respectively.[10,11] The intensity of f^{DE} peak (the area under curve) scales with the film thickness (see also Fig. 5) and it is expected to vanish for a LSMO thickness corresponding to the dead layer, whereas the intensity of the peak at f^{4+} is practically unvaried.[10]

The spectra of the LSMO films terminated with Au capping also reveal two resonance lines approximately at the same frequencies f^{4+} and f^{DE} (red squares in Fig. 4). Since the intensity of the NMR line is proportional to the number of the nuclei in the specific electronic and magnetic states, the change in the Mn^{4+}/Mn^{DE} ratio due to the presence of the gold layer can be measured by NMR directly. As can be seen in Fig. 4, a marked reduction in the Mn^{DE} signal is found in the gold terminated samples, indicating that the capping layer has a direct influence on this specific electronic state (double-exchange state) of the manganite film. The spectroscopic sensitivity of NMR allows detection of quite a large effect already on the thickest structures (12 nm). The reduction is larger for thinner films, as it would be expected in the case Au induces modifications in a constant finite thickness layer in LSMO. The introduction of a thin STO spacer between Au and LSMO layers results in a partial recovery of the Mn^{DE} peak intensity corresponding to an increase in the amount of ions in the Mn^{DE} state (in Fig. 4, the effect of the STO buffer layer is shown only for the 8-nm-thick LSMO layer). However, even in such a case the effect of the gold capping layer on the manganese double-exchange state in the manganite layers is still observed. For the case of the 4-nm-thick LSMO film with the gold capping, the zero-field NMR signal is beyond the sensitivity of our NMR spectrometer and was not detected, revealing that the majority of the LSMO film is in a non-DE state. Notice that this observation does not conflict with the SQUID results, that show the presence of a low-temperature magnetization even for 4 nm of LSMO capped with gold, since manganites may give rise to a variety of insulating ferromagnetic components, such as spin-canted phases, superexchange ferromagnets, or blocked

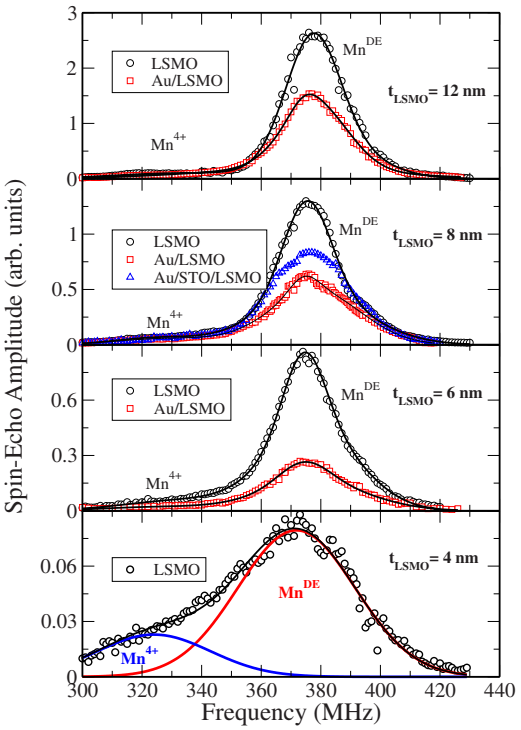

FIG. 4. (Color online) Zero-field ^{55}Mn NMR in various heterostructures: circles—LSMO/STO, squares—Au/LSMO/STO, and triangles—Au/STO/LSMO/STO. The thickness of both the STO buffer layer and Au layer is fixed to be 2 nm while the thickness of the LSMO layer is t_{LSMO}=4, 6, 8, and 12 nm. Solid lines demonstrate the best fit to the experimental data.

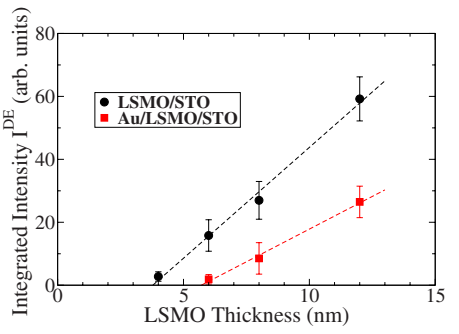

FIG. 5. (Color online) Thickness dependence of the NMR integrated intensity I_{DE} measured in the samples with (squares) and without (circles) gold overlayer.

superparamagnetic clusters. They are not DE phases and their contribution to NMR is negligible while they are still visible in SQUID. The integrated intensity of the Mn^{DE} state, obtained from the fit of the NMR spectra versus LSMO film thickness for the samples with (red squares) and without (black circles) gold show that the critical thickness when the f^{DE} signal disappears is $t_{uncapped} \approx 3.5 \pm 0.3$ nm and $t_{capped} \approx 5.7 \pm 0.4$ nm for gold uncapped and capped LSMO films, respectively (see Fig. 5). We note that this critical thickness $t_{uncapped}$ in uncapped LSMO/STO roughly coincides with the thickness (~3 nm) of the dead layer below which the manganite films appear to be insulating.[16,18] The higher critical thickness in the samples with the gold capping indicates an additional reduction in the amount of the ferromagnetic Mn^{DE} ions at the Au/LSMO interface. Note however that this is only a very rough estimation of the dead-layer thickness, as it relies on the assumption of perfect uniformity in plane, which is not actually the case for the formation of Au nanoparticles.

Finally, it has to be noted that strong changes in the manganite properties could be associated to oxygen vacancies; however if a uniform oxygen deficiency took place in Au/LSMO heterostructures, the positions of the resonance lines would be different. Oxygen deficiency decreases the Mn^{4+} concentration and affects the crystal lattice, reducing the transfer interaction of e_g electrons and weakening the ferromagnetic double-exchange interactions.[34,35] Thus, it is expected to affect the hyperfine interactions of manganese ions measured by NMR.[36] The expected hole concentration (Mn^{4+}) is given by the simple relation $c=0.33-2\delta$, with δ being the concentration of oxygen deficiencies. In order to extract qualitative information about δ we refer to the phase diagram of bulk LSMO,[37] which we will use as a reference although true quantitative analysis based on it might be questionable for thin films. The $\Delta T_C \approx 60$ K measured by SQUID for 6 nm of LSMO with and without Au capping, i.e., on the same samples investigated by NMR, would thus correspond to $\delta=0.05$ and $c \sim 0.2$.

However, such uniform hole concentration would give rise to entirely different zero-field ^{55}Mn NMR spectra.[38,39] As a matter of fact, we did not observe any sizable change in the shape and position of NMR features. If, on the other hand, oxygen vacancies are present but with an inhomogeneus distribution, so that they accumulate in some regions, they could locally drive the transition toward nonferromagnetic phases which are not visible in NMR spectra. In this sense, NMR data are compatible with oxygen vacancies creation only if a strong spatial inhomogeneity in the oxygen content occurs, leading to phase separation between ferromagnetic phases presenting a more or less nominal stoichiometry but reduced T_C with respect to the bulk and nonferromagnetic phases due to the local accumulation of oxygen vacancies.

D. STEM-EELS

In Figs. 6(a) and 6(b), ADF images of a slice containing a gold particle directly in contact with the LSMO layer and the corresponding EELS intensity profiles across the stacking for the various elements of interest are reported as a function of the spatial coordinate (z) perpendicular to the surface. The nominal structure of the sample investigated was: Au(2 nm)/LSMO(6 nm)//STO(001). The EELS data were acquired while displacing the electron beam across the heterostructure. The intensities have been obtained by integrating the signal of the simultaneously acquired O K, Mn $L_{2,3}$, La $M_{4,5}$, Sr $L_{2,3}$, and Au $M_{4,5}$ edges after background subtraction using a power-law fit. Starting from the right (STO substrate side), the intensity profiles extracted from the Mn $L_{2,3}$ and La $M_{4,5}$ fall from 75% down to 25% within one or two unit-cell distances. These data establish an upper limit for any chemical intermixing and, considering the fact that some beam broadening is expected due to specimen finite thickness, they are compatible with the atomically sharp interfaces suggested by the Z-contrast images. At the LSMO/STO interface a clear offset is observed between the La and the Mn signals, with the Mn onset raising a few angstroms after the La signal. Conversely, on the STO side, the Sr signal onset is placed a few angstroms further into the substrate than the Ti onset. This is a clear indication that the LSMO films atomic plane stacking begins with a LaSrO plane, as a consequence of the expected dominant TiO_2 termination of the substrate.

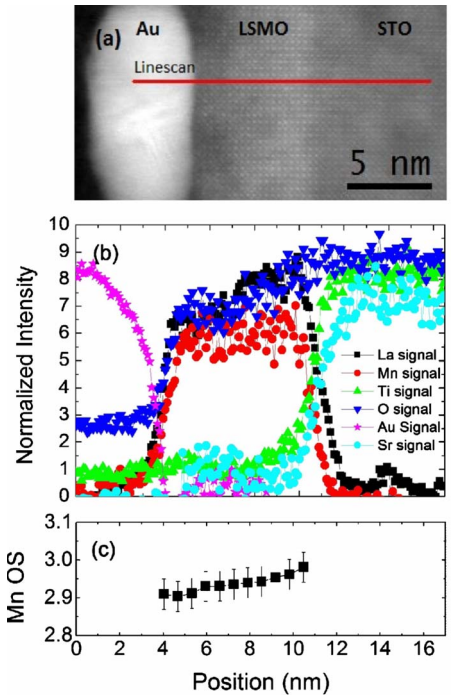

FIG. 6. (Color online) Panel (a): ADF STEM image of a Au nanoparticle on LSMO(6 nm)/STO(001). Panel (b): EELS profiles of the different elements along the line scan indicated in panel (a). La $M_{4,5}$ (black squares), Mn $L_{2,3}$ (red circles), Ti $L_{2,3}$ (green triangles), O K (blue downward triangles), Au $M_{4,5}$ (magenta stars), and Sr $L_{2,3}$ (cyan dots). Panel (c): profile of the Mn oxidation state along the line scan (integrated over 50 nm in direction perpendicular to the line scan) derived from the separation of the prepeak and of the main peak of the O K EELS edge. (See text for details).

The LSMO film surface termination, however, is not so clearly defined, possibly due to some roughening at the Au/

LSMO interface. However the interface between the Au nanoparticles and LSMO is once again very sharp, with the Au, Mn, and La intensities falling down to approximately zero within a few lattice constants. No interdiffusion has been detected in this analysis, confirming previous XPS results.[26] The O signal tails into the regions occupied by the Au nanoparticles could be due to an artifact ensuing from the preparation of the slice (the nanoparticles are embedded in the glue used to prepare the cross sectional sample) but it could also be related to oxygen diffusion in Au. We will discuss this point in more details further below.

It is well known that the line shape of Mn $L_{2,3}$ and O K absorption edges provides information about the Mn oxidation state in mixed-valence manganites.[40] In particular, the O K edge has been proved to be very sensitive to the degree of hybridization between the O $2p$ and Mn $3d$ orbitals, reflecting in a different branching ratio and energy separation between the two peaks of the EELS spectra closest to the onset. In particular, the prepeak right at the onset, around 530 eV arises from transitions into unoccupied O $2p$ final states hybridized with Mn $3d$ states.[40,41] As the t_{2g} band of LSMO is fully occupied, the prepeak has a strong contribution from Mn $3d$ e_g band.[40] It turns out that not only the relative intensity of the prepeak but also the energy separation (ΔE) between the prepeak and the second peak is proportional to the charge transfer from Mn toward oxygen atoms. This kind of relationship has been established looking at the fine structure of O K edge in $La_{1-x}Ca_xMnO_3$ (LCMO) compounds with x variable between 0 and 1, and it allows the Mn OS to be probed directly from O K EELS spectra.[41] Note, however, that other effects, such as structural modifications and consequent changes in the bond angles and orbital overlap, can influence the charge transfer and hybridization between the Mn $3d$ and O $2p$ states. If we apply the calibration of Mn OS determined using the LCMO compounds to the center of an uncapped LSMO/STO(001) sample (data not shown) we obtain a value of $+3.28 \pm 0.04$, very close to what is expected. It is therefore safe to assume that this calibration will provide reasonable numbers for LSMO as well. Accordingly, in Fig. 6(c), the Mn OS arising from the ΔE analysis is plotted as a function of the coordinate z perpendicular to the surface, using a lateral integration window over ~50 nm along the interface (perpendicular to z). A reduced value of the Mn OS is observed through the film: $+2.92 \pm 0.05$ at the LSMO/Au interface, which slightly increases closer to the LSMO/STO interface, up to $+2.96 \pm 0.05$. These values are significantly reduced when compared with the measured OS at the center of the uncapped sample. Interestingly, the STEM-EELS analysis of a structure with a thin STO layer inserted between the LSMO and the Au capping layer indicates once more very sharp interfaces [see Fig. 7(a)] with an intermediate value of the Mn OS in the center of the LSMO film of $+3.15 \pm 0.04$, as shown in Fig. 7(b). There is a clear correspondence between the Mn OS obtained from EELS and the measured suppression of ferromagnetism and conductivity; the deviation from the nominal Mn OS is higher in the LSMO film directly in contact with Au nanoparticles than in the sample with a STO buffer layer and, correspondingly, the suppression of ferromagnetism is higher in the first sample. Finally, it is worth noting that EELS analysis of Au capped LSMO films could not find any distinction between the Mn OS right below Au nanoparticles and those Mn atoms on the free surface. However this is not intrinsic, but probably due to the fact that the slice is much thicker (50 nm) than the typical size of the Au nano particles (7 nm) so that the electron beam probes not only the uncapped LSMO surface seen in the cross section but also some capped zoned underneath, not visible in the Z-contrast image.

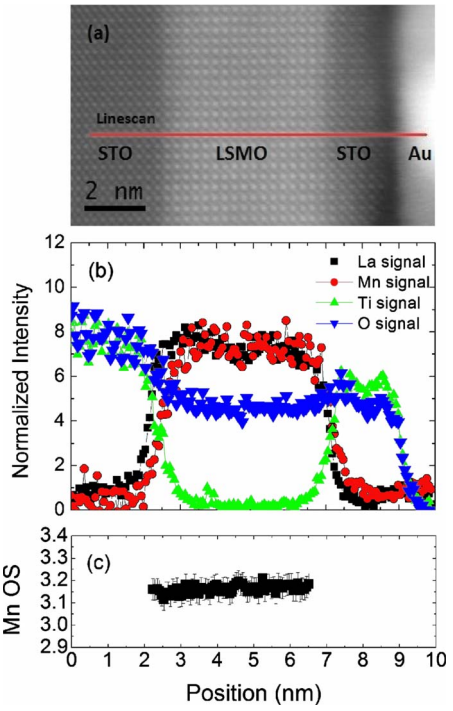

FIG. 7. (Color online) Panel (a): ADF STEM image of a Au nanoparticle on STO(2 nm)/LSMO(6 nm)/STO(001). Panel (b): EELS profiles of the different elements along the line scan indicated in panel (a) La $M_{4,5}$ (black squares), Mn $L_{2,3}$ (red dots), Ti $L_{2,3}$ (green triangles), and O K (blue downward triangles). Panel (c): profile of the Mn oxidation state along the line scan derived from the separation of the prepeak and of the main peak of the O K EELS edge. (See text for details).

E. DFT calculations

In Fig. 8 we compare the site-projected density of states of the Mn atoms in the MnO_2 plane surrounded by La atoms in (i) bulk LSMO, (ii) at the free LSMO surface, and (iii) at the Au/LSMO interface. The latter configuration is shown in the inset of the figure and it results from atomic relaxation of the structure using a conjugate-gradient algorithm. The starting lattice structure of LSMO is that of LSMO grown on STO (choosing the experimental values for in-plane and out-of-plane lattice parameter $a_{\parallel}=3.90$ Å and $a_{\perp}=3.84$ Å, respectively[42]). The epitaxial relation of gold on LSMO was arbitrarily chosen as [100]Au||[100]LSMO, with LSMO terminating with a MnO_2 plane. Therefore, in this case gold is subjected to in-plane compressive strain. Before relaxing the whole structure, the spacing between LSMO and Au has been found by minimizing the total energy as a function of this distance; we found a value of 2.70 Å, giving a first

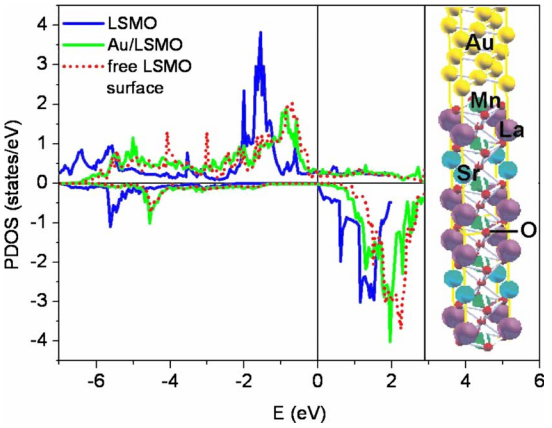

FIG. 8. (Color online) Calculated density of states for Mn placed in the uppermost layer of the LSMO film free and in contact with Au in comparison with bulk DOS of LSMO. The Fermi energy is taken as reference for the energy scale. The structure used in the simulation, corresponding to the [100] axis of Au parallel to the [100] axis of LSMO, is shown on the right.

indication of low chemical interaction between gold and the manganite, as the experimental results show.

When analyzing the figure, we can see a major difference between the bulk and the surface or interfacial DOS. However, the two DOS corresponding to the free and capped LSMO are essentially equivalent, without any sizable change in the alignment of the bands with respect to the Fermi level nor hybridization between LSMO and Au states. Besides, we do not find any magnetic moment transferred to Au atoms. Once again these results indicate a negligible chemical interaction between the two materials, as no net charge transfer and no peculiar line-up of the Fermi level is visible in the DOS. The analysis of the site-projected DOS, details of which will be presented elsewhere, allows us to exclude any effect of charge ordering induced by the proximity of gold different that found at the free surface of LSMO. To conclude, DFT calculations based on an ideal interface and a peculiar epitaxial relationship cannot predict any sizable variation in the electronic properties of the LSMO film induced by the Au capping layer, which appears completely inert.

IV. DISCUSSION

The main question to be addressed here regards the physics responsible for the anomalous effects on the magnetic and transport properties of thin LSMO films upon Au capping. In particular, we should answer the question of whether these effects are due to purely electrostatic effects (with possible potential application concerning the control of the properties of thin LSMO films by electric fields) or additional spurious chemical effects must be taken into account.

The STEM analysis clearly shows that this is not a simple two-dimensional (2D) problem, as the Au initial wetting is not continuous but occurs via deposition of nanoparticles. This growth mode causes an intrinsic inhomogeneity in the film. Simple models considering the LSMO film as made of a homogeneous internal layer with bulk physical properties sandwiched between a "dead layer" at the interface with the STO substrate and an additional "magnetically dead layer" at the top Au/LSMO interface are clearly inappropriate to describe a much more complex system with a true three-dimensional structure. It is well known that phase separation is a typical phenomenon of manganite thin films[43] and in the present case we expect it to play a dominant role due to the inhomogeneous Au coverage. As a matter of fact, the strong increase in the resistivity due to the formation of Au particles on top could be easily interpreted in terms of separation of the film in ferromagnetic conductive phases (spatially localized in the zones of the films not covered by Au nanoparticles) and nonferromagnetic insulating phases below Au nanoparticles. This picture would be coherent with NMR data showing a decrease in the relative weight of the double-exchange phases upon Au deposition, without modification of the corresponding line shape. Such a phase separation could occur with grains of more or less nominal LSMO and other electronic phases where double exchange is completely suppressed (not visible anymore in NMR spectra). Upon capping of Au nanoparticles, the conduction takes place via percolation of conductive phases, according to what has been observed in other phase separated films (Ref. 43 and references therein). The nature of the nonconductive phases is not well identified but the combination of SQUID and NMR data clearly indicate that they are not ferromagnetic.[44]

Unfortunately the fine structure of a film exhibiting phase separation on the nanometer scale is not accessible to STEM-EELS analysis because the typical size of the Au nanoparticles (6 nm) and most likely, the ensuing phase separation, is much smaller than the thickness of the specimen used in the experiment (~30 nm along the electron-beam direction). In these conditions, the electron beam averages LSMO zones with and without Au on top and consequently averages any physical behavior characterized by shorter length scales. Nevertheless we observe that the averaged Mn OS state is quite constant as a function of the distance from the Au/LSMO interface (see Figs. 6 and 7). This is another indication of the inadequacy of the 2D model in which we would expect the presence of an interfacial "additional magnetic dead layer." In the presence of such layer a clear variation in the Mn OS profile close to the LSMO/Au interface should be noticed, regardless of the physical reason underlying the phenomenon. Now, taking into account the unavoidable integration along the thickness of the slice, EELS data could be consistent with a phase separated film with grains at least 4–6 nm in size extending through the film.

Coming back to the physical origin of this phase separation, we first consider the possibility of charge injection/depletion in the manganite due to the Au/LSMO interface formation. In a very simple model, this phenomenon should depend on the difference of the work functions between Au and LSMO, which are, respectively, 5.1 eV and 4.7 eV for bulk samples. For these values, we would expect a net transfer of electrons from LSMO to Au. In consequence, the hole doping of the LSMO should increase, explaining the suppression of magnetism and conductivity. However, an estimate of the perturbation of the initial density of carriers in LSMO (10^{21} cm^{-3}) (Ref. 2) caused by a difference in the

work function of 0.4 eV gives a relative variation on the order of 6% of the interfacial carrier density, falling down to zero over a distance on the order of a lattice constant, if we assume a Thomas-Fermi screening length of 0.2 nm. Referring to the phase diagram of bulk $La_{(1-x)}Sr_xMnO_3$ and, in particular, to the dependence on x of T_C,[37] this doping variation would change T_C just a few kelvin, which is not compatible with the observed variation of 185 K for 4-nm-thick LSMO films covered by Au nanoparticles. Furthermore, the sign of the injected charge in LSMO predicted on the basis of the work functions is not compatible with EELS data showing a decrease in the Mn OS state upon Au capping. In fact electron depletion in LSMO takes place via depletion of Mn $3d$ e_g states, thus leading to an increase in the concentration of Mn^{4+}. The subsequent increase in the Mn OS is opposite to the experimental findings, so we can conclude that charge transfer between Au and LSMO is not the driving force for the observed huge suppression of ferromagnetism and conductivity. Note that the consideration of the variation in the Au work function in nanoparticles with respect to bulk cannot invalidate the previous conclusion: in fact, the work function increases by reducing the size of the nanoparticles[45] so that the sign of the charge transfer due to the work-function difference cannot change when considering the granular structure of the Au film. As a final remark, we mention the results of field effect experiments on ultrathin LSMO films both with top[46] and side[16] gate configuration probing the perturbation on ferromagnetism and conductivity by charge injection. All published data demonstrate that only small variations in T_C or metal-insulator transition temperature (a few kelvin) can be achieved, for electric fields up to the limit of the breakdown of the STO layer used as insulator between the LSMO electrode and the gate. This is an additional proof of the fact that charge injection cannot explain the anomalous suppression of ferromagnetism and conductivity observed in the present case.

Looking for different electrostatic effects, we next consider the perturbation of fundamental electrostatic parameters like the Hubbard energy or transfer integrals in the manganite due to screening effects by the Au nanoparticles. Similar phenomena have been indeed found in the case of thin films of NiO capped with Ag, where an enhancement of the exchange energy takes place after capping with silver, thus producing an increase in the Néel temperature of the antiferromagnet.[15] This was attributed to the screening of electrostatic interactions in NiO produced by image charges representing the presence of an equipotential plane at the Ag/NiO interface, thus leading to the reduction in the Hubbard energy (U) and of the charge-transfer energy (Δ) associated to the creation of the configurations $d^{n+1}d^{n-1}$ and p^5d^{n+1}, respectively. However, we note that in the present case we are not dealing with an insulating material but with LSMO (a "bad metal" with a density of carriers on the order of 10^{21} cm^{-3}). Proximity effects, like those produced in the case of Ag on NiO by the image charges in Ag, should be limited to a very small screening length in case of LSMO so that it is hard to figure out a sizable perturbation on the overall magnetic properties of a 6-nm-thick film. Furthermore, contrary to the case of Ag/NiO, the sign of the variation in T_C due to possible image charge screening is not in agreement with experiments. A simple theory establishing a relationship between Δ, U, and the Curie temperature has been proposed by Zhao,[47] who suggested that doped holes mainly reside on oxygen orbitals d-p exchange and electron-phonon coupling can better explain the physics of manganites instead of double exchange. According to this theory, ferromagnetic interaction between adjacent Mn ions then results from the antiferromagnetic exchange interaction between Mn ions and the oxygen hole (spin $\frac{1}{2}$) sitting in between while the overall ferromagnetic exchange energy between the two Mn ions is $J \propto t_{pd}{}^4/\Delta^3$ where t_{pd} is a hybridization matrix element between the d and p orbitals and Δ is the charge-transfer energy. A reduction in Δ should then reflect in the increase in the exchange energy and consequently of T_C; on the contrary, we experimentally assist to the decrease in T_C upon gold capping. Furthermore, local-density approximation calculations do not show any sizable change in the energy separation between O $2p$ states and unoccupied Mn $3d$ states, which is related to Δ. It clearly appears that proximity effects cannot explain the huge suppression of ferromagnetism and conductivity presented in this work.

At this point it is worthwhile noting that strain effects can be ruled out since we did not find any preferential epitaxial relationship between the LSMO layer and Au nanoparticles, whose area of contact with the LSMO substrate is indeed very limited (see Sec. III C). Therefore, the simplest explanation of the observed phenomena is the formation of oxygen vacancies leading to a composition $La_{0.66}Sr_{0.33}MnO_{3-\delta}$ upon deposition of Au nanoparticles on top of LSMO. In fact, oxygen vacancies should produce an effect similar to chemical doping, altering the Mn OS$=3.33-2\delta$ similarly to a doping of $x=0.33-2\delta$. The experimentally observed decrease in the Mn OS down to +2.94 for the Au/LSMO interface and +3.15 for the Au/STO 2 nm/LSMO heterostructure is compatible with values of δ of 0.195 and 0.08, respectively, corresponding to variations in the oxygen stoichiometry of approximately 6.5% and 2.7% in each case. These variations are clearly within the experimental errors of our previous XPS measurements, and also of the present EELS measurements, so that we cannot provide a direct proof of sample deoxygenation. Nevertheless, on the basis of the bulk phase diagram of LSMO they could largely explain the anomalous decrease in T_C upon Au capping. The expected T_C in a bulk LSMO sample for a doping of $x=0.17$, which is the value obtained for the sample Au/STO(2 nm)/LSMO(6 nm), is about 250 K, to be compared with $T_C=300$ K from SQUID data on 6 nm of LSMO. In the case of Au/LSMO x should be negative (−0.16) thus definitely entering the antiferromagnetic portion of the phase diagram. Note that a negative value of x could be only associated to some Mn^{2+} ions, which, to our knowledge, have been only detected at free LSMO surfaces after annealing in vacuum.[48] The information on the Mn OS is averaged in the volume of the LSMO so that a nominal value of +2.92 is most probably associated to the coexistence of zones with more or less nominal LSMO and other zones with strongly deoxygenated LSMO, corresponding to the presence of Au nanoparticles above. The average T_C measured by SQUID should correspond to the magnetic behavior of the first zones.

Also measurements of the magnetization M_0 of LSMO films previously presented in Ref. 18 are in qualitative agree-

ment with this model based on deoxygenation of LSMO induced by Au capping: our data show indeed a clear reduction in the magnetization upon Au capping. Upon capping a 4 nm LSMO film with 2 nm of Au we reported a reduction in M_0 from 420 ± 70 to 150 ± 100 emu/cm^3. Finally note that the detrimental effect of the proximity of Au nanoparticles on the LSMO properties is maintained also for higher nominal coverage of Au (data not shown), when it forms a continuous film. In this case we observed a coherent high reduction in T_C along with significant damage in the manganite layer under the electron-beam irradiation taking place during TEM analysis, which is often observed in deoxygenated perovskites. The scenario is then coherent with a higher deoxygenation in samples with a thick, continuous gold capping, corresponding to the interaction of the entire LSMO surface with Au nanoparticles. An irreversible oxygen depletion in the manganite due to the high reactivity of the nanoparticles takes place at the early stage of the film formation and persists when a continuous layer of gold is formed.

The final issue is how to explain such a strong deoxygenation at the Au/LSMO interface and also how this phenomenon could survive after insertion of a STO buffer layer 2 nm thick. At variance with continuous Au films, the reactivity of Au nanoparticles is well known and indeed they are used as catalysers like Pt particles in some applications.[45] Furthermore, the oxidation of Au nanoparticles has been already investigated by other authors,[49] so a local diffusion of oxygen atoms from LSMO to Au during the formation of Au nanoparticles is largely possible. The final ingredient for solving this puzzle is the explanation of how this phenomenon could work with an intermediate buffer layer of STO. Note that STO is much more stable than LSMO against oxygen losses[50] which are however largely possible, leading for instance to conductive STO after annealing in vacuum. It is then reasonable to assume that Au nanoparticles can pump oxygen from STO. Oxygen could then migrate from LSMO to STO due to the higher stability of the latter, eventually creating oxygen vacancies in the LSMO film, though not directly in contact with Au. Clearly this phenomenon becomes less and less relevant when increasing the thickness of the STO buffer layer, which becomes an efficient barrier to interdiffusion. As a matter of fact, we found that for 6 nm of STO buffer layer (data not shown) there is no variation in the T_C of the LSMO film upon Au capping.

V. CONCLUSIONS

In summary, we have investigated the huge suppression of ferromagnetism and conductivity in LSMO films capped with gold. We found that for low Au nominal thicknesses, Au nanoparticles are formed, causing a sizeable reduction in the Mn oxidation state, which we attribute to an inhomogeneous deoxygenation of the manganite underneath. This finding explains the large decrease in conductivity, which is due to worsened percolation of metallic regions through insulating, nonferromagnetic phases. We have excluded the possibility of a purely electrostatic effect (charge injection depletion and of screening of electrostatic interactions in the manganite) underlying these phenomena. On the contrary, we suggest that the high chemical reactivity of Au nanoparticles can account for the partial deoxygenation of LSMO below the Au nanoparticles, thus providing nucleation centers for different electronic phases. The ensuing phase separation within the film explains the suppression of ferromagnetism and conductivity. These findings should be taken into account when explaining the different functionalities in metal-oxide interfaces in highly correlated oxide heterostructures.

ACKNOWLEDGMENTS

The authors are deeply grateful to Marco Leone for his skillful technical assistance, to Julia Luck for specimen preparation for STEM, and to Masashi Watanabe for the plug in for principal component analysis in digital micrograph. This work has been partially funded by Consorzio Nazionale Interuniversitario per le Scienze Fisiche della Materia (CNISM) as part of a Progetto d'Innesco della Ricerca Esplorativa 2005. Work at ORNL (M.V.) was supported by the Division of Materials Sciences and Engineering of the U.S. Department of Energy. C. Magen acknowledges financial support from the Spanish Ministry for Science and Education. A.A. Sidorenko and R. De Renzi acknowledge support of EU STREP Grant No. NMP3-CT-2006-033370—OFSPIN.

*Present address: Instituto de Nanociencia de Aragón-ARAID and Departamento de Física de la Materia Condensada, Universidad de Zaragoza, 50009 Zaragoza, Spain.

[1] For a review, see C. H. Ahn, A. Bhattacharya, M. Di Ventra, J. N. Eckstein, C. D. Frisbie, M. E. Gershenson, A. M. Goldman, I. H. Inoue, J. Mannhart, A. J. Millis, A. F. Morpurgo, D. Natelson, and J.-M. Triscone, Rev. Mod. Phys. **78**, 1185 (2006).

[2] W. Prellier, P. Lecoeur, and B. Mercey, J. Phys.: Condens. Matter **13**, R915 (2001).

[3] A. M. Haghiri-Gosnet, T. Arnal, R. Soulimane, M. Koubaa, and J. P. Renard, Phys. Status Solidi A **201**, 1392 (2004).

[4] M. Viret, M. Drouet, J. Nassar, J. Contour, C. Fermon, and A. Fert, Europhys. Lett. **39**, 545 (1997).

[5] M. Bowen, M. Bibes, A. Barthélémy, J.-P. Contour, A. Anane, Y. Lemaître, and A. Fert, Appl. Phys. Lett. **82**, 233 (2003).

[6] V. A. Vas'ko, V. A. Larkin, P. A. Kraus, K. R. Nikolaev, D. E. Grupp, C. A. Nordman, and A. M. Goldman, Phys. Rev. Lett. **78**, 1134 (1997).

[7] J. M. De Teresa, A. Barthélémy, A. Fert, J. P. Contour, R. Lyonnet, F. Montaigne, P. Seneor, and A. Vaurés, Phys. Rev. Lett. **82**, 4288 (1999).

[8] L. Fratila, I. Maurin, C. Dubourdieu, and J. C. Villégier, Appl. Phys. Lett. **86**, 122505 (2005).

[9] V. Dediu, M. Murgia, F. C. Matacotta, C. Taliani, and S. Barbanera, Solid State Commun. **122**, 181 (2002).

[10] A. A. Sidorenko, G. Allodi, R. De Renzi, G. Balestrino, and M.

Angeloni, Phys. Rev. B **73**, 054406 (2006).
[11] M. Bibes, Ll. Balcells, S. Valencia, J. Fontcuberta, M. Wojcik, E. Jedryka, and S. Nadolski, Phys. Rev. Lett. **87**, 067210 (2001).
[12] J. Z. Sun, D. W. Abraham, R. A. Rao, and C. B. Eom, Appl. Phys. Lett. **74**, 3017 (1999).
[13] A. Tebano, C. Aruta, S. Sanna, P. G. Medaglia, G. Balestrino, A. A. Sidorenko, R. De Renzi, G. Ghiringhelli, L. Braicovich, V. Bisogni, and N. B. Brookes, Phys. Rev. Lett. **100**, 137401 (2008).
[14] Y. Konishi, Z. Fang, M. Izumi, T. Manako, M. Kasai, H. Kuwahara, M. Kawasaki, K. Terakura, and Y. Tokura, J. Phys. Soc. Jpn. **68**, 3790 (1999).
[15] S. Altieri, M. Finazzi, H. H. Hsieh, M. W. Haverkort, H.-J. Lin, C. T. Chen, S. Frabboni, G. C. Gazzadi, A. Rota, S. Valeri, and L. H. Tjeng, Phys. Rev. B **79**, 174431 (2009).
[16] I. Pallecchi, L. Pellegrino, E. Bellingeri, A. S. Siri, D. Marré, A. Tebano, and G. Balestrino, Phys. Rev. B **78**, 024411 (2008).
[17] H. J. A. Molegraaf, J. Hoffman, C. A. F. Vaz, S. Gariglio, D. van der Marel, C. H. Ahn, and J.-M. Triscone, Adv. Mater. (Weinheim, Ger.) **21**, 3470 (2009).
[18] R. Bertacco, S. Brivio, M. Cantoni, A. Cattoni, D. Petti, M. Finazzi, F. Ciccacci, A. A. Sidorenko, M. Ghidini, G. Allodi, and R. De Renzi, Appl. Phys. Lett. **91**, 102506 (2007).
[19] S. Brivio, M. Cantoni, D. Petti, A. Cattoni, R. Bertacco, M. Finazzi, F. Ciccacci, A. Sidorenko, G. Allodi, M. Ghidini, and R. De Renzi, Mater. Sci. Eng., B **144**, 93 (2007).
[20] Y. A. Boikov and T. Claeson, Phys. Rev. B **70**, 184433 (2004).
[21] G. Allodi, A. Banderini, R. De Renzi, and C. Vignali, Rev. Sci. Instrum. **76**, 083911 (2005).
[22] E. A. Turov and M. P. Petrov, *Nuclear Magnetic Resonance in Ferro- and Antiferromagnets* (Halsted, New York, 1972).
[23] G. Kresse and J. Furthmüller, Phys. Rev. B **54**, 11169 (1996).
[24] H. J. Monkhorst and J. D. Pack, Phys. Rev. B **13**, 5188 (1976).
[25] P. E. Blöchl, O. Jepsen, and O. K. Andersen, Phys. Rev. B **49**, 16223 (1994).
[26] D. Petti, A. Cattoni, S. Brivio, M. Cantoni, R. Bertacco, and F. Ciccacci, J. Appl. Phys. **103**, 044903 (2008).
[27] The gain in the total free energy due to condensation is $kT \ln(P/P_0)$, where P is the pressure due to the impinging beam of evaporated atoms and P_0 the vapour pressure at the temperature of the substrate. This terms favors layer-by-layer growth if the supersaturation ratio (P/P_0) is greater than unity. This is exactly our case as growth of Au particles takes place at RT, with a deposition rate of a few angstroms per minute and at a base pressure in the 10^{-10} Torr range. The formation of nanoparticles is then clearly related to the strong difference in the surface and interface free energies.
[28] A. J. Millis, Nature (London) **392**, 147 (1998); K. H. Ahn, T. Lookman, and A. R. Bishop, *ibid.* **428**, 401 (2004); C. Thiele, K. Dörr, O. Bilani, J. Rödel, and L. Schultz, Phys. Rev. B **75**, 054408 (2007); A. Tebano, C. Aruta, P. G. Medaglia, F. Tozzi, G. Balestrino, A. A. Sidorenko, G. Allodi, R. De Renzi, G. Ghiringhelli, C. Dallera, L. Braicovich, and N. B. Brookes, *ibid.* **74**, 245116 (2006).
[29] R. Bertacco, M. Riva, M. Cantoni, L. Signorini, and F. Ciccacci, Appl. Phys. Lett. **86**, 252502 (2005).
[30] G. Matsumoto, J. Phys. Soc. Jpn. **29**, 606 (1970).
[31] G. Allodi, M. Cestelli Guidi, R. De Renzi, and M. W. Pieper, J. Magn. Magn. Mater. **242-245**, 635 (2002).
[32] P. A. Algarabel, J. M. De Teresa, J. Blasco, M. R. Ibarra, C. Kapusta, M. Sikora, D. Zajac, P. C. Riedi, and C. Ritter, Phys. Rev. B **67**, 134402 (2003).
[33] M. M. Savosta and P. P. Novák, Phys. Rev. Lett. **87**, 137204 (2001).
[34] S. V. Trukhanov, L. S. Lobanovski, M. V. Bushinsky, V. A. Khomchenko, N. V. Pushkarev, I. O. Troyanchuk, A. Maignan, D. Flahaut, H. Szymczak, and R. Szymczak, Eur. Phys. J. B **42**, 51 (2004).
[35] N. Abdelmoula, K. Guidara, A. Cheikh-Rouhou, E. Dhahri, and J. C. Joubert, J. Solid State Chem. **151**, 139 (2000).
[36] A. M. DeLeon-Guevara, P. Berthet, J. Berthon, F. Millot, A. Revcolevschi, A. Anane, C. Dupas, K. Le Dang, J. P. Renard, and P. Veillet, Phys. Rev. B **56**, 6031 (1997).
[37] A. Urushibara, Y. Moritomo, T. Arima, A. Asamitsu, G. Kido, and Y. Tokura, Phys. Rev. B **51**, 14103 (1995).
[38] G. Allodi, R. De Renzi, G. Guidi, F. Licci, and M. W. Pieper, Phys. Rev. B **56**, 6036 (1997).
[39] G. Papavassiliou, M. Pissas, M. Belesi, M. Fardis, M. Karayanni, J. P. Ansermet, D. Carlier, C. Dimitropoulos, and J. Dolinsek, Europhys. Lett. **68**, 453 (2004).
[40] M. Varela, M. P. Oxley, W. Luo, J. Tao, M. Watanabe, A. R. Lupini, S. T. Pantelides, and S. J. Pennycook, Phys. Rev. B **79**, 085117 (2009).
[41] W. Luo, M. Varela, J. Tao, S. J. Pennycook, and S. T. Pantelides, Phys. Rev. B **79**, 052405 (2009).
[42] F. Tsui, M. C. Smoak, T. K. Nath, and C. B. Eom, Appl. Phys. Lett. **76**, 2421 (2000); M. Huijben, L. W. Martin, Y.-H. Chu, M. B. Holcomb, P. Yu, G. Rijnders, D. H. A. Blank, and R. Ramesh, Phys. Rev. B **78**, 094413 (2008).
[43] E. Dagotto, T. Hotta, and A. Moreo, Phys. Rep. **344**, 1 (2001).
[44] By SQUID we observed a reduction in the saturation magnetic moment in LSMO films capped with Au, which means that the missing Mn^{DE} signal in NMR is at least partially associated to nonferromagnetic phases.
[45] N. S. Phala and E. van Steen, Gold Bull. **40**, 150 (2007).
[46] S. Brivio, D. Petti, M. Cantoni, and R. Bertacco (unpublished).
[47] Guo-meng Zhao, Phys. Rev. B **62**, 11639 (2000).
[48] M. P. de Jong, I. Bergenti, V. A. Dediu, M. Fahlman, M. Marsi, and C. Taliani, Phys. Rev. B **71**, 014434 (2005).
[49] D. C. Lim, I. Lopez-Salido, R. Dietsche, M. Bubek, and Y. D. Kim, Surf. Sci. **600**, 507 (2006).
[50] H. Kumigashira, A. Chikamatsu, R. Hashimoto, M. Oshima, T. Ohnishi, M. Lippmaa, H. Wadati, A. Fujimori, K. Ono, M. Kawasaki, and H. Koinuma, Appl. Phys. Lett. **88**, 192504 (2006).